science.sciencemag.org/content/369/6500/161/suppl/DC1

# Supplementary Materials for

## Structure and selectivity engineering of the $M_1$ muscarinic receptor toxin complex

Shoji Maeda*, Jun Xu, Francois Marie N. Kadji, Mary J. Clark, Jiawei Zhao, Naotaka Tsutsumi, Junken Aoki, Roger K. Sunahara, Asuka Inoue, K. Christopher Garcia, Brian K. Kobilka*

*Corresponding author. Email: shojim@stanford.edu (S.M.); kobilka@stanford.edu (B.K.K.)

Published 10 July 2020, *Science* **369**, 161 (2020)
DOI: 10.1126/science.aax2517

**This PDF file includes:**

## Materials and Methods

### Expression and purification

A synthetic DNA fragment encoding the muscarinic toxin 7 (MT7) amino acid sequence (UniProt ID: Q8QGR0) was made by assembling primers by PCR and was cloned into pFastBac1 (ThermoFisher Scientific) with N-terminal GP67-signal sequence, MBP-, and His-tags followed by an HRV-3C protease cleavage site. Baculovirus was made according to the manufacturer's instruction, and Hi5 cells (Expression Systems) were infected at a density of 3.5-4.0 million $ml^{-1}$. Media were harvested 60-72 hours of post infection, supplemented with 5 mM $CaCl_2$, 1 mM $NiSO_4$, 20 mM Tris-HCl pH 7.5, and protease inhibitors and incubated at room temperature for 40 minutes. Following the removal of the precipitation by centrifugation, MT7 was purified by a Ni-chelating sepharose chromatography and a size-exclusion chromatography (SEC) column. Purified MT7 was concentrated to over 1 mM and flash frozen. The human $M_1$AChR fused with T4L in the ICL3 was derived from the previous crystallographic study (*21*) with S112R mutation introduced to thermostabiliize the receptor (*44*). Baculovirus was made according to the manufacturer's manual, and Sf9 cells (Expression Systems) were infected at a density of 3.5-4.0x million $mL^{-1}$ in the presence of 10 μM atropine (Sigma-Aldrich). Cells were harvested 48 to 60 hours post infection. Receptors were extracted from insect cell membrane by n-dodecyl-β-D-maltoside (DDM, Anatrace) and purified by Ni-chelating sepharose chromatography in the presence of 10 μM atropine. Eluted receptors were further purified by M1 FLAG affinity chromatography and SEC in the presence of atropine with the detergent exchanged to Lauryl-maltose neopentyl glycol (LMNG, Anatrace). Purified receptor was mixed with excess MBP-MT7 and HRV-3C protease, and incubated for overnight at 4˚C. Protein was

loaded over an amylose column to remove free MBP-tag or uncleaved MBP-MT7. Flow-through from the amylose column was concentrated and further purified by SEC to remove excess MT7 and HRV-3C protease. Peak fractions were concentrated and used for crystallization at 10-20 mg $ml^{-1}$. The human $M_2$AChR was expressed and purified essentially in the same way as $M_1$AChR.

**Crystallization**

Purified $M_1$AChR-MT7 was crystalized by the hanging drop vapor diffusion method. Crystals were grown in 22-27% SOKALAN PA 25 CL (Molecular Dimensions), 0.1 M HEPES-Na pH 7.5, 0.1 M NaCl, appeared after 2-5 days and reached to the full size in 2 weeks. Crystals were flash frozen in liquid nitrogen with 10% glycerol as a cryo-protectant.

**Data collection, and structure determination**

X-ray diffraction data were collected on the GM/CA beamline 23ID-D at the Advanced Photon Source, Argonne National Laboratories. Data were collected with 0.5 s exposures and 0.5˚ oscillations. Diffraction data were processed using XDS (*45*) and aimless (*46*). The structure was solved by molecular replacement using Phaser (*47*). For the input model, the inactive $M_1$AChR structure (PDB ID: 5CXV) was split into the receptor and T4L components and used as separate search models. For MT7, manually adjusted monomeric MT7 structure (PDB ID: 2VLW) was used as a search model. The resulting model was completed by an iterative refinement using phenix.refine in Phenix suite (*48*) and manual building with Coot (*49*). MolProbity was used for structure validation. Crystallographic statistics are reported in Supplementary Table 1.

**Pull-down assay**

For the clone24 or Tx24 pull-down assay, either 3 μM $M_1$AChR or $M_2$AChR in 100 μL buffer (20 mM HEPES-Na pH7.5, 100 mM NaCl, 0.01% LMNG, 3 mM $CaCl_2$, 10 μM iperoxo or 10 μM atropine) was incubated with or without 5 μM Tx24 for 30 min at room temperature and loaded over an M1-FLAG column. The column was washed with the buffer and eluted with the elution buffer (20 mM HEPES-Na pH7.5, 100 mM NaCl, 0.01% LMNG, 5m M EDTA, 200 μg/ml FLAG peptide, 10 μM iperoxo or 10 μM atropine). Eluted protein was analysed by SDS-PAGE.

**Construction of the phage library, selection and purification of 1st generation toxin clone24**

The coding sequence of MT7 was cloned into the pADL-23c phagemid vector (Antibody Design Laboratories, San Diego, USA) by the Gibson Assembly method. Randomized sequences were introduced into each finger loop one after another by the PCR amplification of the entire phagemid using Q5 polymerase (NEB). Each primer used for the randomization is phosphorylated at the 5' end in order for the efficient ligation. In the first randomization of finger loop 2, deletion up to four residues is additionally introduced. The PCR product was treated with DpnI for 2 hours and then purified by the agarose gel. The purified DNA fragment was ligated using the DNA Ligation Kit Mighty Mix (Takara) for 4 hours to overnight. The ligated DNA was purified by the ethanol precipitation and dissolved in water. The resulting randomized phagemid DNA was electroporated into the TG-1 electrocompetent cells (Lucigen) and the cells were plated onto 15 cm square or round LB plates supplemented with 100 μg $ml^{-1}$ ampicillin and 0.1% glucose. The colonies were harvested into 2xYT medium with 100 μg $ml^{-1}$ ampicillin and 0.1% glucose. The cells were diluted into 1L of 2xYT medium with 100 μg $ml^{-1}$ ampicillin and 0.1% glucose to make absorption at 600 nm (A600) around 0.1 and grown at 37°C at 225 rpm.

When A600 reached 0.8 to 0.9, 8.9x 10^13 helper phages were added and further incubated at 37°C at 225 rpm for 30 min. The cells were spun down and resuspended into 1L of 2xYT supplemented with 100 μg $ml^{-1}$ of ampicillin and 25 μg $ml^{-1}$ of kanamycin, and incubated at 30°C at 225 rpm for overnight. The media was harvested by centrifugation at 4000 rpm for 15 min, mixed with 1/4 volume of phage precipitation buffer consisting of 20% PEG8000 and 1.5 M NaCl. Following incubation on ice for 1h, the mixture was centrifuged at 11,000 g for 30 min to precipitate the phage. The phage was dissolved into PBS, spun down to precipitate bacterial cell debris. The supernatant was harvested and phage precipitation was repeated. The re-precipitated phage was dissolved into PBS, supplemented with 50% glycerol and flash frozen. The rest of the harvested TG-1 cells were split into two parts and grown for 1-2h at 37°C at 225 rpm to recover. One half of the cells were spun down and resuspended into 2xYT supplemented with 25% glycerol, and flash frozen. The second half was used for the Maxi-prep to purify phagemid DNA. This phagemid DNA was used as a template for the next round of finger loop 3 randomization. Finally, finger loop 1 randomization was introduced into the post finger loop 3 randomized phagemid. For the panning against $M_2$AChR, the biotinylated receptor prepared using EZlink-NHS-PEG4-biotin (Thermo Fisher Scientific) was immobilized on the streptavidin MagneSphere Paramagnetic Particles (Promega). The receptor-bound beads were incubated with phage for 45 min at room temperature in the phage display buffer consisting of 20 mM HEPES pH 7.5, 100 mM NaCl, 0.5% BSA, 0.05% LMNG, 0.005% CHS, 10 μM atropine. The beads were washed with the phage display buffer and phage were eluted by 0.1 M glycine (3.0). The selected clones were transferred to a modified pMAL vector. Engineered toxins in pMAL vector were expressed in Rosetta2(DE3) (Novagen) in TB media supplemented with 100 μg $ml^{-1}$ ampicillin and 34 μg/ml chloramphenicol. Harvested cells were incubated in the 2.5 mL $g^{-1}$ cells

of TES buffer (0.2 M Tris-HCl pH 8.0, 0.5 mM EDTA, 0.5 M Sucrose) for 45 min, then diluted with 5mL $g^{-1}$ cells of 1/4 diluted TES buffer and further incubated for 45 min. The cells were spun down at 20,000 g for 15 min. The supernatant was supplemented with 2 mM $MgCl_2$ and incubated with 2 mL $L^{-1}$ culture of Ni-sepharose resin for 1h. The resin was washed with a high salt wash buffer consisting of 20 mM HEPES-Na pH 7.5, 500 mM NaCl, 20 mM imidazole pH 8.0 and a low salt wash buffer consisting of 20 mM HEPES-Na pH 7.5, 100 mM NaCl, 20 mM imidazole pH 8.0. The protein was eluted with the low salt wash buffer supplemented with 300 mM imidazole pH 8.0 and further purified by SEC. For the cellular assay, NMR measurement, and radioligand binding assay, the Ni-sepharose purified protein was treated with HRV-3C protease and dialyzed against 20 mM HEPES(7.5), 100 mM NaCl for overnight at 4°C. The protein was spun down to remove the precipitation and loaded over a Ni-sepharose column to trap toxin protein and remove cleaved MBP. After eluting from the column, residual free MBP and uncleaved MBP-toxin was removed by running through an amylose column and flow through was collected. The protein was further purified by SEC. The toxin peak was collected, concentrated to over 700 μM, supplemented with 10% glycerol, and stored at -80°C until use.

**Construction of yeast surface display library and affinity maturation of clone24**

A mutant library of clone24 was generated by PCR amplification of the coding region of the toxin using the error-prone polymerase from the Genemorph II kit (Agilent). The fragment was amplified twice using the product of the first PCR reaction as a template for the second round, which yields the average error rate of ~6 mutations/gene. The PCR products were then scaled up using Q5 polymerase (New England Biolabs) and primers with an extension that contains homology to the pCT3CBN vector, a derivative of pCT302. Agarose gel-purified PCR products

were combined with linearized pCT3CBN vector DNA and the DNA mixture was electroporated into EBY100 yeast that yielded 2x10^7 transformants. Electroporated yeast cells were amplified in SDCAA selection media and induced in SGCAA induction media. In order to enrich high-affinity binders, 4x10^8 yeast from the error-prone library were stained with 500 nM $M_2$AChR labeled with anti-M1 FLAG antibody conjugated with Alexa Fluor 647 in yeast binding buffer (20 mM HEPES pH7.5, 100 mM NaCl, 0.05% LMNG, 0.005% CHS, 5 mM $CaCl_2$, 0.1% BSA, 10 mM Maltose, 10 μM atropine). Stained yeasts were mixed with anti-Alexa647 conjugated magnetic microbeads (Miltenyi) and loaded onto a Magnetic Activated Cell Sorting (MACS) LS column (Miltenyi) to isolate binders. The enriched yeasts were amplified in SDCAA, induced in SGCAA, and the selection was repeated in the same way but using 1x 10^8 cells and 20 nM $M_2$AChR. In the 3rd round selection, we used Fluorescence Activated Cell Sorting (FACS) to further enrich high-affinity binders. Induced post 2nd yeast was stained with 20 nM $M_2$AChR labeled with anti-M1 FLAG antibody conjugated with Alexa647 as well as anti-Myc antibody conjugated with Alexa488, in order to assess the expression levels of the engineered toxin clones. These stained yeast cells were sorted using SH800S cell sorter (SONY) based on the expression and binding to $M_2$AChR. Over 200,000 cells were collected in the 3rd selection and amplified in SDCAA. The 4th round selection was performed in the same way as the 3rd round but with more stringent gating in the FACS sorting giving around 100,000 yeast cells collected. The post 4th selection cells were amplified and 50 clones were randomly sequenced to find the mutations contributing to the maturation. The consensus mutations were combined to make Tx24 and the synthetic gene fragment with a C-terminal His-tag (Integrated DNA Technologies) was cloned into pMAL vector for the bacterial expression, and pFastBac1 vector with N-terminal GP67 secretion sequence and MBP-tag for the insect expression. Tx24 was expressed and

purified in the same protocol as clone24 from the bacterial expression system and the same protocol as MT7 from the insect expression system. The amino-acid sequences of MT7, clone24, and Tx24 are provided in the fig. S10. The expression plasmid for these engineered toxins are available upon request.

**On-yeast affinity measurement**

The coding region of clone24 or Tx24 was each cloned into the pCT3CBN vector and transformed into EBY100. The transformed yeast cells were grown in SDCAA media and the surface expression was induced in SGCAA media for 48 hours. The cells were washed twice with a buffer containing 20 mM HEPES-Na pH 7.5, 100 mM NaCl, 0.1% BSA, 0.05% LMNG, 3 mM $CaCl_2$ 10mM maltose with no ligand, 10 μM atropine, 10 μM NMS, 10 μM tiotropium, or 1 mM acetylcholine and incubated with $M_2$AChR pre-incubated with respective condition at each concentration for 30 min at room temperature. The cells were washed twice with the cold buffer and incubated with anti-FLAG antibody labeled with Alexa647 for 10 min at 4°C. Following the anti-FLAG staining, the cells were washed twice with the cold buffer and the fluorescence signal was analysed by BD Accuri C6 flow cytometer (BD biosciences). The receptor-bound fraction was normalized with the highest value to 1.0 within the clones and fit by a Sigmoidal curve using Prism 8.0 (GraphPad Software Inc., San Diego).

**NanoBiT-G-protein dissociation assay**

GPCR-induced G-protein activation was measured by a NanoBiT-G-protein dissociation assay (*40*), in which interaction between a Gα subunit and a Gβγ subunit was monitored by a NanoBiT system (Promega). Specifically, a NanoBiT-G protein consisting of a large fragment (LgBiT)-

containing Gα subunit ($G\alpha_{i1}$ for $M_2$AChR, $M_4$AChR and MOR; $G\alpha_s$ for β2AR; $G\alpha_q$ for $M_1$AChR, $M_3$AChR and $M_5$AChR) and a small fragment (SmBiT)-fused $G\gamma_2$ subunit (C68S-mutant) was expressed together with untagged $G\beta_1$ subunit and with or without a test GPCR. HEK293 cells were seeded in a 10-cm culture dish at a concentration of $2 \times 10^5$ cells $mL^{-1}$ (10 mL per well in DMEM (Nissui) supplemented with 10% fetal bovine serum (Gibco), glutamine, penicillin and streptomycin) 1-day before transfection. Transfection solution was prepared by combining 20 µL (per dish hereafter) of polyethylenimine solution (Polysciences; 1 mg $mL^{-1}$) and a plasmid mixture consisting of 500 ng LgBiT-containing Gα subunit, 2.5 µg $G\beta_1$, 2.5 µg C68S-mutant SmBiT-fused $G\gamma_2$ (C68S), and 1 µg a test GPCR (or pCAGGS empty plasmid) in 1 mL of Opti-MEM (ThermoFisher Scientific). To enhance expression of NanoBiT-G protein, 500 ng of RIC8A and RIC8B was co-transfected with NanoBiT-Gq and NanoBiT-Gs, respectively. After incubation for 1 day, transfected cells were harvested with 0.5 mM EDTA-containing Dulbecco's PBS, centrifuged and suspended in 8 mL of HBSS containing 0.01% bovine serum albumin (BSA; fatty acid–free grade; SERVA) and 5 mM HEPES (pH 7.4) (assay buffer). The cell suspension was dispensed in a white 96-well plate at a volume of 60 µL per well and loaded with 20 µL of 50 µM coelenterazine (Carbosynth) diluted in the assay buffer. To measure PAM activity of Tx24 toward antagonist, the following procedure was performed. After 1-h incubation at room temperature, titrated antagonist (Atropine for $M_{1\text{-}5}$AChR; NMS or Tiotropium for $M_2$AChR; Naloxone for MOR; Propranolol for β2AR) diluted in the assay buffer at 10X of final concentration was added at a volume of 10 µl per well. After 30-min incubation, Tx24 diluted in the assay buffer at 10X of final concentration was added at a volume of 10 µl per well and incubated for 30 min. The plate was measured for baseline luminescence (Spectramax L, Molecular Devices) and a test agonist (20 µL; 10 µM Acetylcholine for M1-5; 1 µM DAMGO

for MOR; 1 μM Isoproterenol for β2AR) were manually added. To measure antagonist activity of Tx24, 10 μL of the assay buffer was added in place of the antagonist and the cells were pretreated with titrated Tx24 (0.1-2 μM) before addition of a test agonist (1 μM Acetylcholine for M1-5; 100 nM DAMGO for MOR; 100 nM Isoproterenol). To measure agonistic activity of Tx24, 20 μL of the assay buffer was added in place of the antagonist and Tx24 pretreatment before luminescent measurement. After incubation for 3-5 minutes at room temperature, the plate was read for the second luminescent measurement. The second luminescence counts were normalized to the initial count and fold-change signals over vehicle treatment were used to plot G-protein dissociation response. Using Prism 8 software (GraphPad Prism), the G-protein dissociation signals were fitted to a four-parameter sigmoidal concentration-response curve, from which $pIC_{50}$ values (negative logarithmic values of $IC_{50}$ values) were used to calculate mean and SEM. A change in a Tx24-treated $pIC_{50}$ value from a control $pIC_{50}$ value ($\Delta pIC_{50}$) were calculated for each experiment and used for statistical analyses. The allosteric parameter (α) was calculated by using a pre-installed equation of Prism 8 ("Allosteric EC50 shift, X is log(concentration)") in which we constrained a $LogK_B$ parameter equal to -7.51 and used four antagonist-titrated data (Tx24 concentrations of 0, 100 nM, 500 nM and 2 μM) .

**Bimane fluorescence sensor assay**

The $M_2$AChR bimane construct was designed to probe the movement of TM6 taking advantage of a tryptophan/bimane quenching technique (*50*). Distances between Cα of $Ser210^{5.62}$ and $Thr386^{6.34}$ in the inactive (PDB 3UON) and active (PDB 4MQS) structures of $M_2$AChR are 6.1 and 11.5 Å, respectively (Fig. S14), which are an optimal range of tryptophan-based quenching of the bimane fluorescence (5-15Å). $Ser210^{5.62}$ and $Thr386^{6.34}$ are mutated to tryptophan and

cysteine, respectively, based on an $M_2$AChR minimal-cysteine construct (C124S, C439A, C443S, C457L, C274A, C324A, C337A). Cys386 shows predominant labeling by monobromobimane (mBBr) compared with the minimal-cysteine construct. M1 FLAG affinity chromatography purified $M_2$AChR (~10 μM) was mixed with 0.6 mM monobromobimane and incubated on ice for 3 h. The fluorophore-labeled receptor was then purified by a size-exclusion chromatography to remove excess monobromobimane. The purified protein was concentrated to 93 μM, flash-frozen with liquid nitrogen and stored at -80°C until use. Fluorescence spectroscopy experiments were performed on a Fluolog Fluorometer (Horiba). The excitation and emission band-pass were set to 4 nm. The final protein concentrations were 200 nM for $M_2$AChR, 1 μM for Tx24, and 1 μM for Nb9-8. The reaction buffer contains 20 mM HEPES, pH 7.5, 100 mM NaCl, 0.005% LMNG, 0.0005% CHS with no ligand, 10 μM atropine, or 1 mM acetylcholine. All experiments were performed at 22°C.

**NMR measurement of $M_2$AChR-Tx24**

The $^{13}CH_3$-ε-methionine labeled $M_2$AChR was expressed, labeled and purified as described previously (*42*). Briefly, the Sf9 cells were grown in methionine-deficient medium and infected at a density of $4x10^6$ $ml^{-1}$ with $M_2$AChR baculovirus in the presence of 10 μM atropine and $^{13}CH_3$-ε-methionine at a concentration of 250 mg $L^{-1}$, and then incubated for 48 hours at 27 ℃. The receptor was purified by Ni-NTA chromatography, M1 FLAG affinity chromatography and size exclusion chromatography and finally exchanged to a $D_2O$-based buffer containing 20 mM HEPES-Na pH 7.5, 100 mM NaCl, 0.01% LMNG, 0.003% CHS. The receptor was concentrated to around 85 μM and subjected to NMR experiments. For Tx24-bound state spectrum, Tx24 was added into the apo-state receptor at around 1.5:1 molar ratio. For atropine-bound state spectrum,

~1 mM atropine was added into the apo-state receptor. For atropine+Tx24-bound spectrum, Tx24 was further added to the atropine-bound receptor at around 1.5:1 molar ratio. All NMR samples were loaded into the Shigemi microtubes for data collection at 25 ℃ on a Bruker Avance 800 MHz spectrometer equipped with a triple-resonance cryogenic probe. The $^{1}$H-$^{13}$C heteronuclear single-quantum coherence (HSQC) spectra were recorded with spectral widths of 12820.5 Hz in the $^{1}$H-dimension (w1) and 16077.2 Hz in the $^{13}$C-dimension (w2) centered at 45 ppm in $^{13}$C-dimension. For all spectra, 512 x 128 complex points were recorded and a relaxation delay of 2 s were inserted to allow spin to relax back to equilibrium. 80 scans gave rise to an acquisition time around 12 h for each spectrum. All NMR spectra were processed using the software package NMRPipe/NMRDraw (*51*) and analyzed using the program NMRViewJ (*52*).

**Dissociation binding kinetics with clone24**

The initial radioligand binding assay was performed using Sf9 membrane expressing $M_2$AChR. The membrane suspension in a buffer containing 20 mM Tris-HCl pH 7.5, 100 mM NaCl, 10 mM $MgCl_2$, 0.5 % BSA was first incubated with 1 nM of [$^{3}$H]NMS for 120 min at room temperature, then either 1 μM of purified clone24, or an equivalent volume of buffer was added and further incubated for 60 min at room temperature. Dissociation was triggered by adding 10 μM atropine at each time point. The dissociation was stopped by rapid filtration of the membrane and the receptor-bound [$^{3}$H]NMS was monitored by a scintillation counter (Beckman Colter).

**Dissociation binding kinetics with Tx24**

Dissociation studies using [$^{3}$H]NMS (Perkin Elmer) were performed in membranes (5 μg per point) prepared from CHO cells expressing wildtype human $M_1$, $M_2$, $M_3$, $M_4$, or $M_5$AChR, as

previously described (*53*). For the $\beta_2$AR, a stable cell line (HEK293) expressing the $\beta_2$AR was used. Briefly, membranes were incubated with 0.3 nM [$^3$H]NMS in assay buffer (20 mM HEPES, pH 7.4, 100 mM NaCl) for 1 h at room temperature in the absence or presence of 2 μM Tx24. To initiate [$^3$H]NMS dissociation, an equal volume of excess atropine was added (final concentration of 50 μM to prevent re-association of [$^3$H]NMS). For the $\beta_2$AR membranes (5 μg per point) were incubated with 0.5 nM [$^3$H]dihydroalprenolol ([$^3$H]DHAP, Perkin Elmer) in assay buffer (20 mM HEPES, pH 7.4, 100 mM NaCl) for 1 h at room temperature in the absence or presence of 2 μM Tx24. Propranolol (10 mM) was used to initiate [$^3$H]DHAP dissociation from $b_2$AR. Samples were harvested at various times by rapid filtration on GF/C Unifilter™ (Perkin Elmer) 96-well plates followed by three wash steps with ice cold assay buffer. Filters were dried and incubated with scintillation cocktail (MicroScintO™, Perkin Elmer). [$^3$H]NMS or [$^3$H]DHAP was measured by liquid scintillation counting using a TopCount™ (Perkin Elmer). Dissociation constants were determined using Prism 6.0 (GraphPad Software Inc., San Diego), based on a single-phase exponential decay.

**Pharmacological Tx24 Affinity Estimations**

To evaluate the relative affinity of Tx24 for $M_1$AChR, $M_2$AChR or closely related $M_4$AChR, membranes from CHO cells (5 μg per point) expressing the MAChR isoforms were co-incubated with [$^3$H]NMS (0.3 nM) in the presence of various concentrations of Tx24. Samples were incubated for 2 hr at room temperature in assay buffer (20 mM HEPES, pH 7.4, 100 mM NaCl, 10 mM $MgCl_2$, 2 μM GTPγS). 50 μM atropine was used to define non-specific binding. The reaction was terminated by rapid filtration on GF/C Unifilter™ (Perkin Elmer) 96-well plates followed by three wash steps with ice cold assay buffer. Filters were dried and incubated with

scintillation cocktail (MicroScintO™, Perkin Elmer) and [$^3$H]NMS or [$^3$H]DHAP was measured by liquid scintillation counting using a TopCount™ (Perkin Elmer). Data were fit to a logistics curve using Prizm 6 (GraphPad LLC, San Diego CA). To analyze the apparent biphasic curve on the $M_2$AChR, the rising phase of [$^3$H]NMS binding was fitted separately from the falling phase were fit separately.

**Saturation isotherms with [$^3$H]NMS on $M_2$AChR**

Membranes (5 µg per point) from CHO cells stably expressing the $M_2$AChR (*53*) were incubated with increasing concentrations of [$^3$H]NMS in assay buffer (20 mM HEPES, pH 7.4, 100 mM NaCl, 10 mM $MgCl_2$, 2 µM GTPγS) in the presence or absence of 0.5 µM Tx24 for 24 hr at room temperature. Atropine (50 µM) was used to define non-specific binding. The [$^3$H]NMS binding was terminated by rapid filtration on GF/C Unifilter™ (Perkin Elmer) 96-well plates followed by three wash steps with ice-cold assay buffer. Filters were dried and incubated with scintillation cocktail (MicroScintO™, Perkin Elmer) and [$^3$H]NMS or [$^3$H]DHAP was measured by liquid scintillation counting using a TopCount™ (Perkin Elmer). Affinity measurements were determined using Prism 6.0 (GraphPad Software Inc., San Diego), based on a one-site saturation model.

**[$^{35}$S]GTPγS Binding**

Membranes from CHO cells expressing wildtype human $M_2$AChR, as described above, were pretreated with 120 µM GDP (final assay concentration 30 µM) in assay buffer (20 mM HEPES, pH 7.4, 100 mM NaCl, 10 mM $MgCl_2$) for 20 min at room temperature. Then membranes (15-35 µg per well) were incubated for 1 h at 30ºC with 100 pM [$^{35}$S]GTPγS and increasing

concentrations of the agonist, acetylcholine, in the absence or presence of 1 μM Tx24. Bound [$^{35}$S]GTPγS was separated from free nucleotide using rapid filtration on GF/C Unifilter™ 96-well plates and measured by scintillation counting as described above. $EC_{50}$s were determined using Prism 6.0 (GraphPad Software Inc., San Diego).

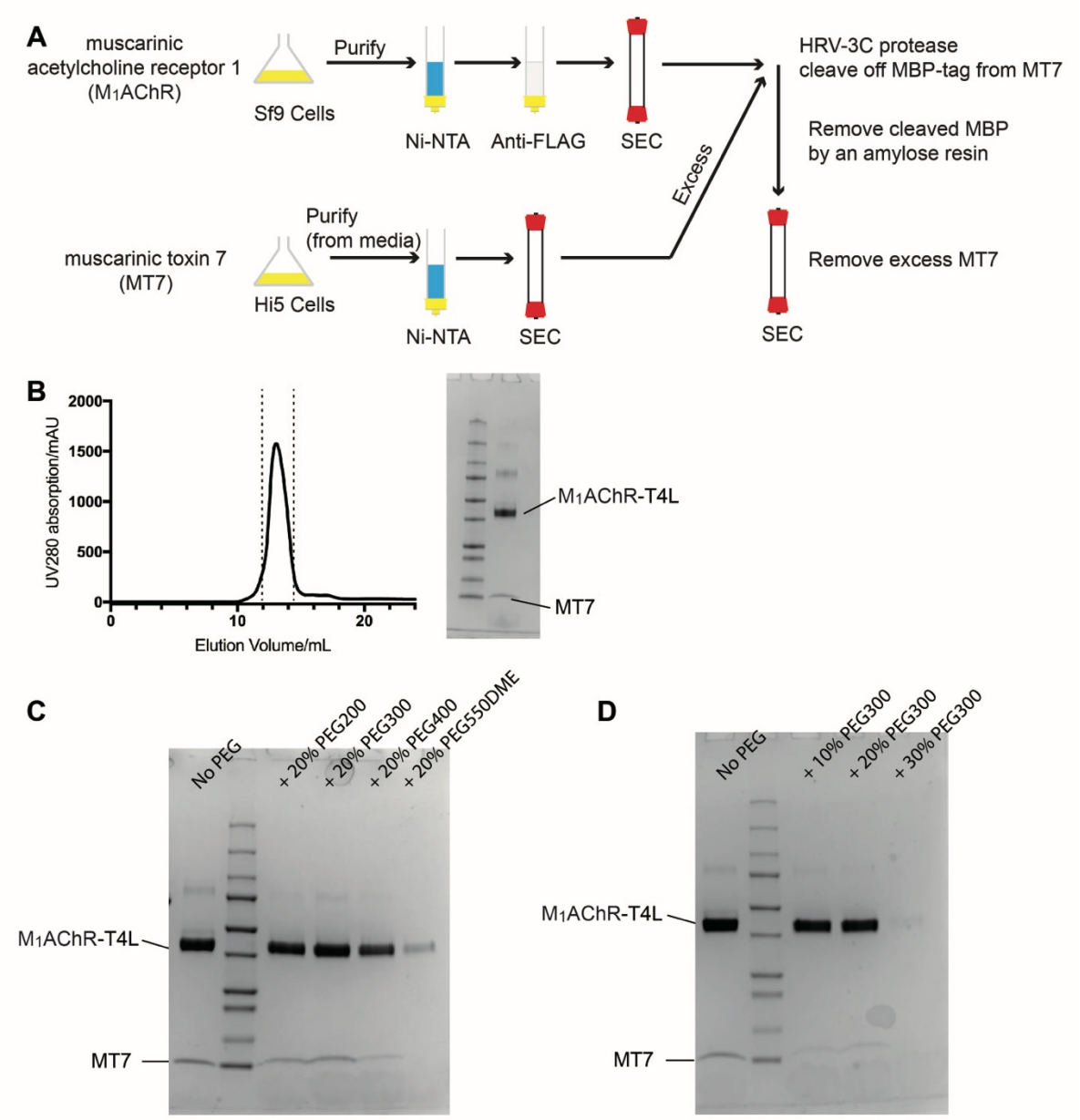


**Fig. S1. (A)** Purification scheme for the $M_1$AChR-MT7 complex. Atropine is present through the entire $M_1$AChR purification process as well as $M_1$AChR-MT7. **(B)** Monodisperse peak profile of the preparative size-exclusion chromatography (SEC) of $M_1$AChR-MT7 complex. The peak fraction indicated between dashed lines was analyzed by SDS-PAGE to confirm the presence of MT7 together with $M_1$AChR. Atropine is present throughout the purification process at 10 µM. **(C, D)** Pull-down assay of $M_1$AChR-MT7 in the presence of low-molecular weight PEG molecules commonly used in the protein crystallization.

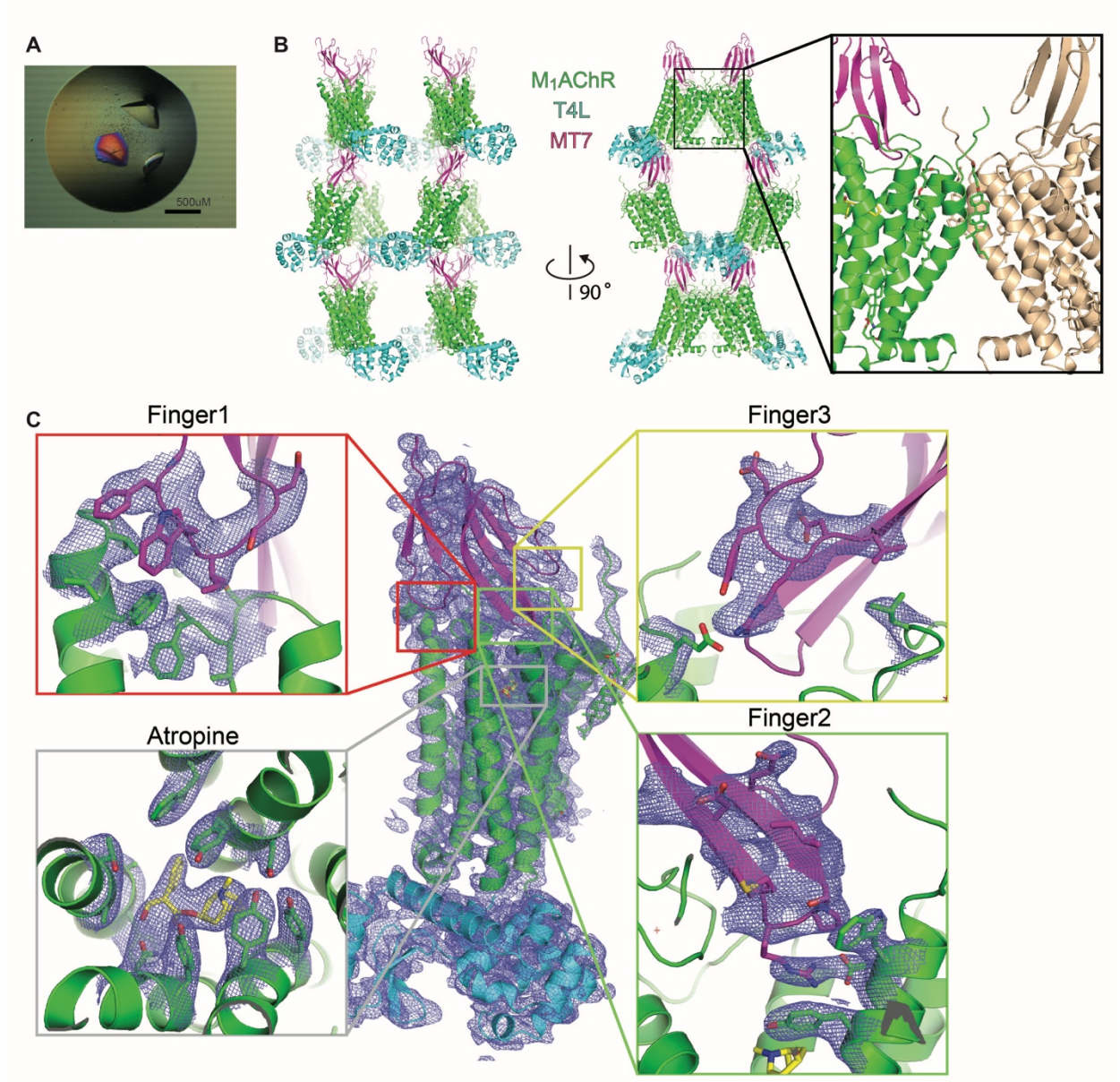


**Fig. S2. (A)** Representative picture of the $M_1$AChR-MT7 crystals in the hanging drop. Scale bar indicates 0.5 mm. **(B)** Crystal packing of the $M_1$AChR-MT7 complex. A kink in TM1 is likely a consequence of a crystal contact at TM1 as shown in an enlarged window with the neighboring molecule colored in pale brown for clarity. (**C**) Electron density map of the $M_1$AChR-MT7 complex. The overall density map around the complex is shown in the middle panel. The density at each finger loop and around the orthosteric binding pocket are shown in enlarged windows. Maps are contoured at 1.0 σ.

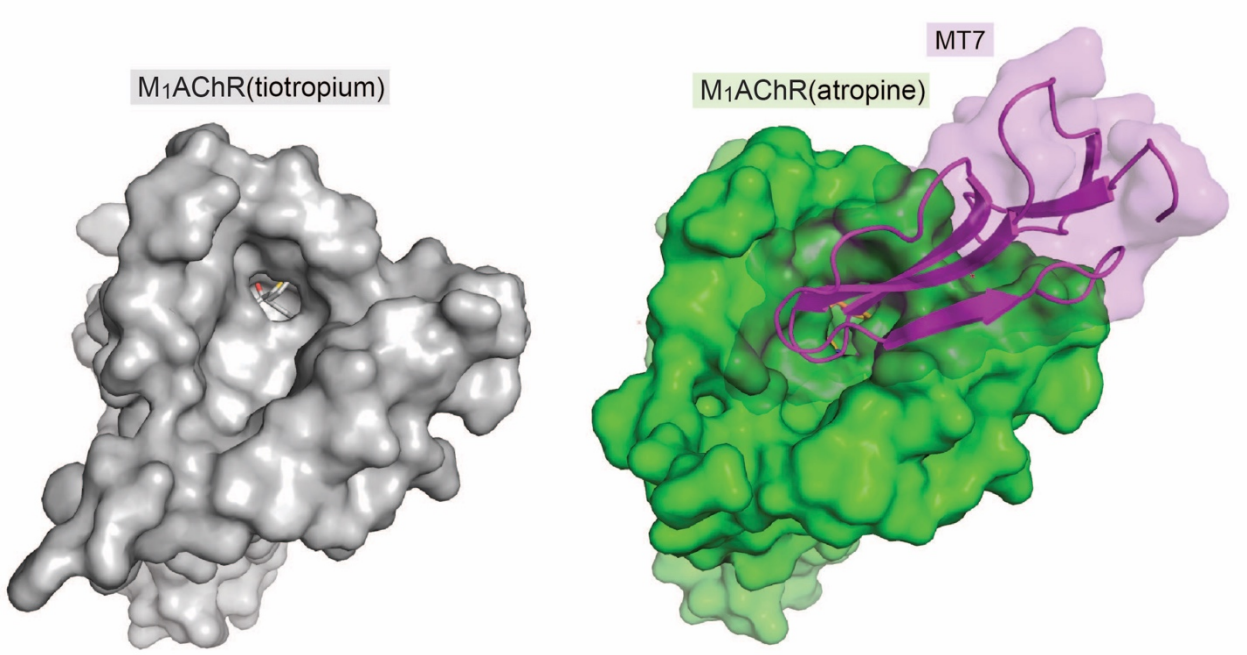


**Fig. S3.** MT7 occludes the orthosteric site of $M_1$AChR. The orthosteric site of $M_1$AChR is open to the extracellular vestibule (left). MT7 occupies the extracellular allosteric site and occludes the entrance to the orthosteric site (right).

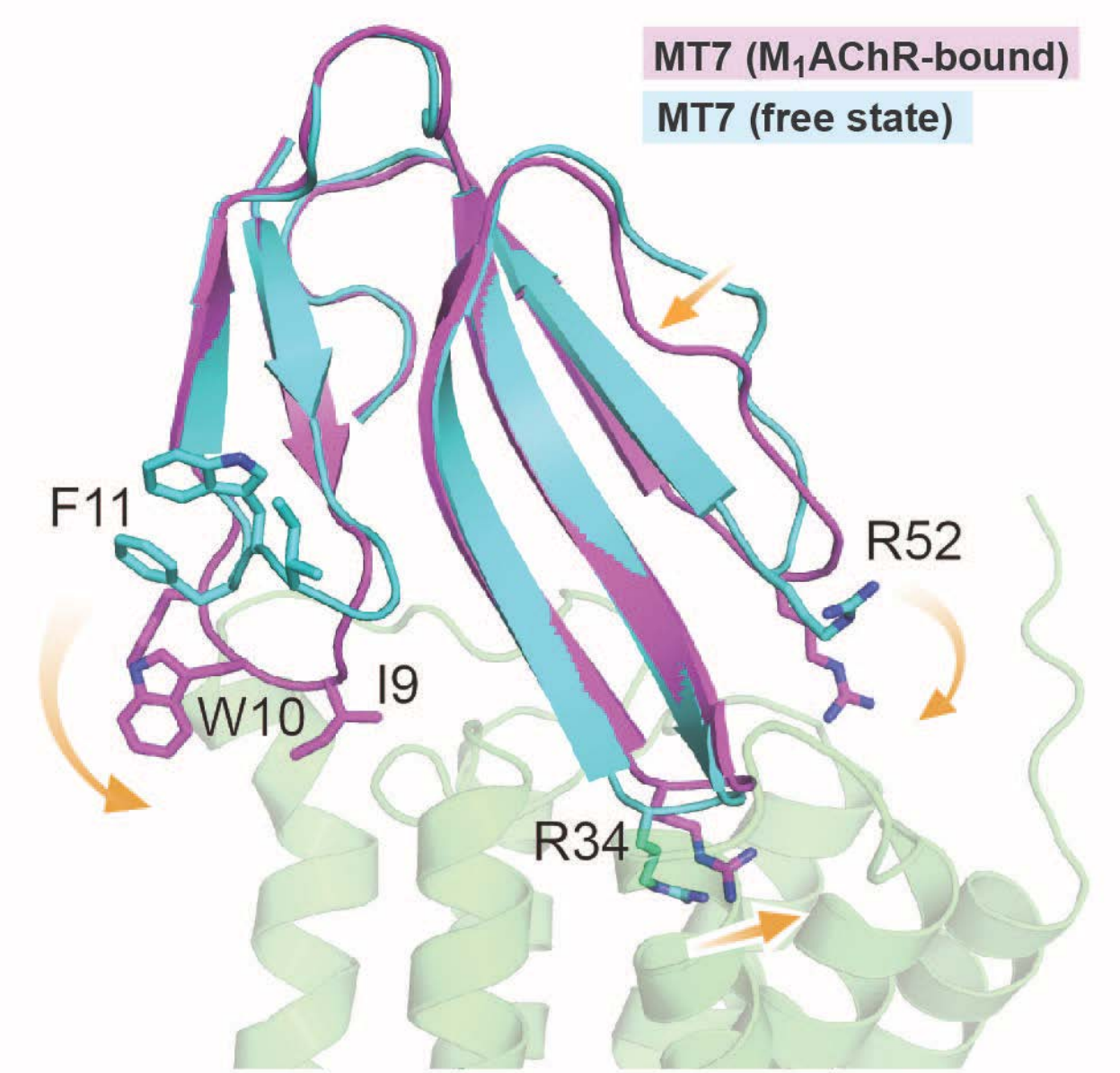


**Fig. S4.** Conformational change of MT7 upon binding to $M_1$AChR. Structure of MT7 in its free state (cyan, PDB ID: 2VLW) is superposed onto MT7 (magenta) in the $M_1$AChR-MT7 complex. Conformational changes are indicated with orange arrows with the representative side-chain residues shown as sticks.

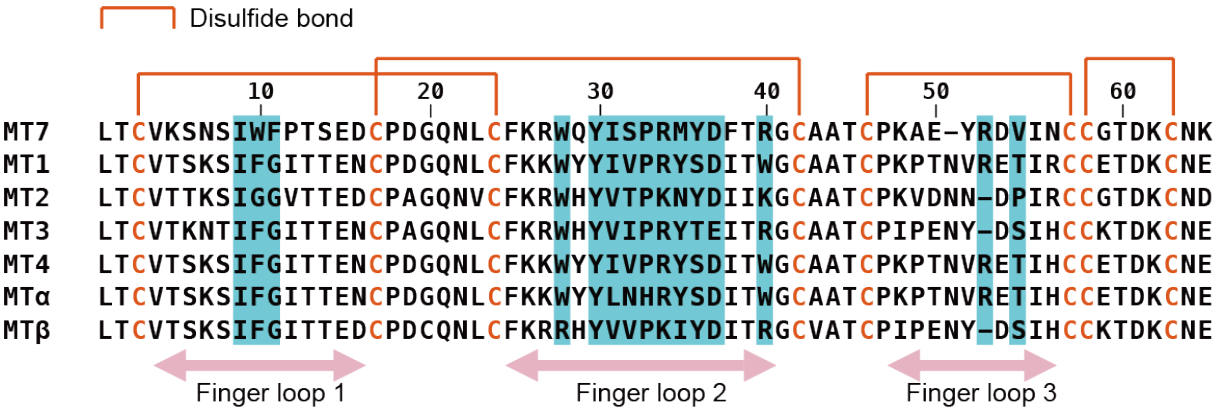


**Fig. S5.** Sequence alignment of muscarinic toxins. Disulfide-forming cysteine residues are colored in orange with disulfide pairings indicated by orange lines. Residues in MT7 that make interaction with $M_1$AChR and equivalent residues in family members are highlighted by cyan boxes. Each finger loop region is indicated with double-sided arrows.

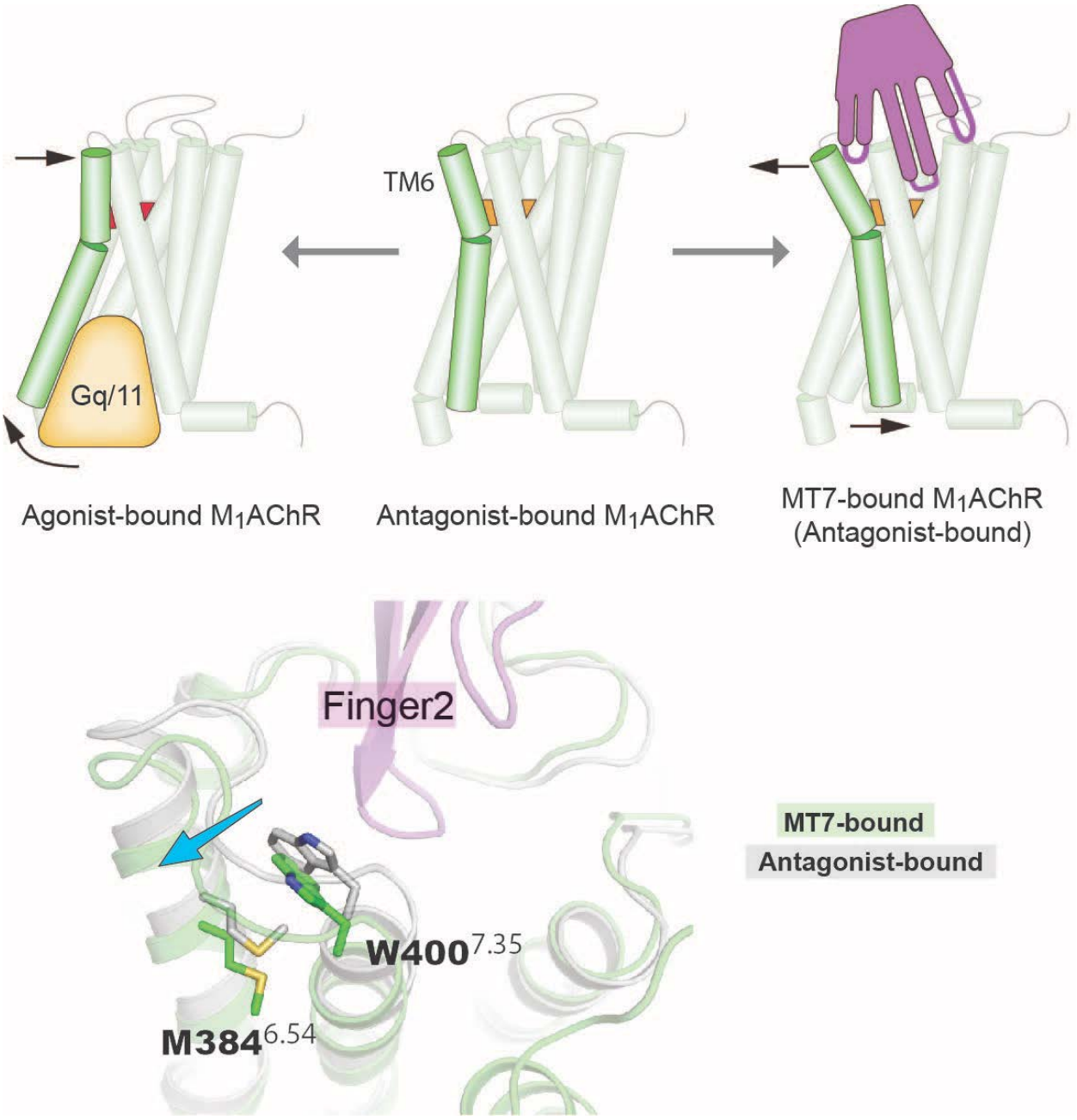


**Fig. S6.** Structural changes in $M_1$AChR stabilized by MT7. The intracellular side of TM6 opens outward upon activation by agonist to accommodate the signaling molecule such as G protein or arrestin. Upon antagonist binding, this TM6 outward movement is suppressed with the extracellular side fixed open. Binding of MT7 causes the outward movement of TM6 at the extracellular side that is coupled with the inward movement of TM6 in the intracellular side.

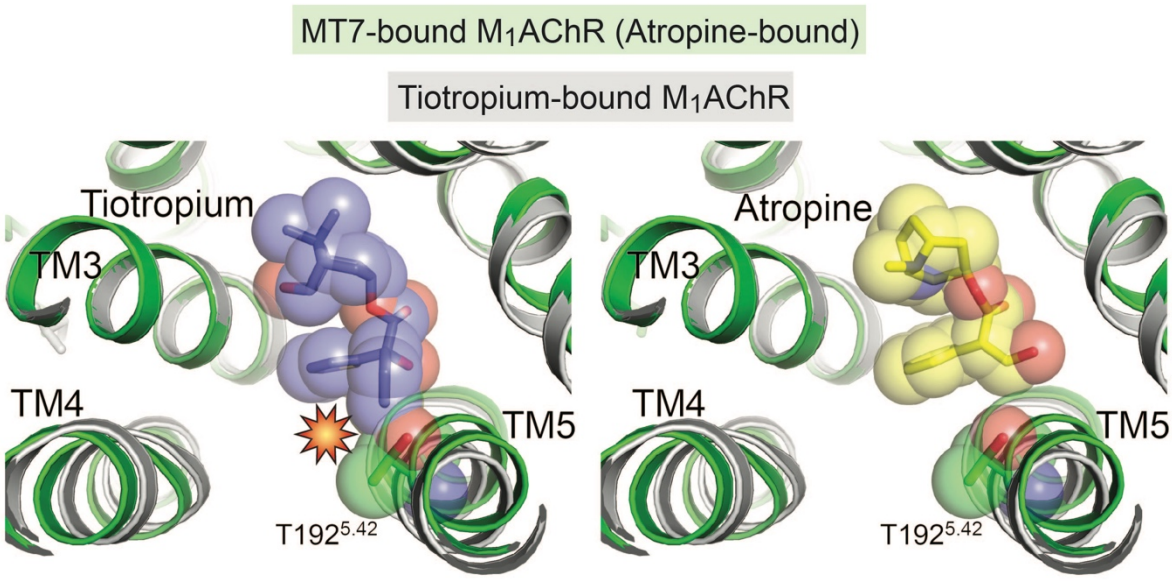


**Fig. S7.** Small inward displacement of TM5 in the atropine-bound $M_1$AChR (green, this study) compared to the tiotropium-bound structure (grey, PDB ID: 5CXV). Note that a 2-thienyl group in tiotropium clashes with the side-chain of T192 when superposed in the atropine-bound $M_1$AChR.

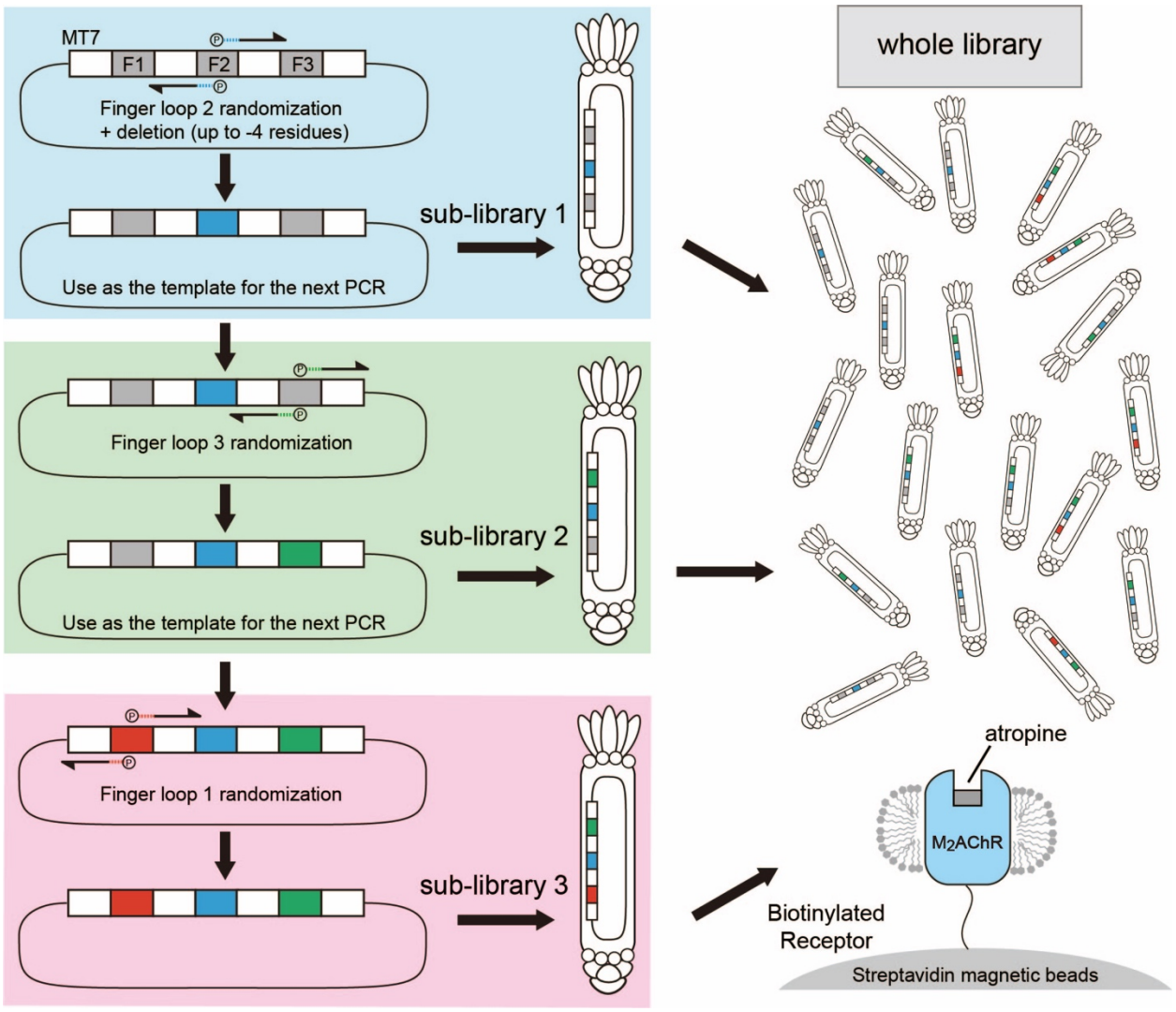


**Fig. S8.** Phage display library construction scheme. Random mutation was introduced into the part of finger loop 2 interacting with $M_1$AChR. Up to 4 residue deletion was included in this region. In the subsequent step, random mutation was introduced into finger loop 3 using the plasmid product of the first library as a template. In the final round, random mutation was introduced in finger loop 1 using the plasmid product of the second-round randomization. Phage sub-libraries were made using the transformants from each randomization step and the mixture was used for the selection against $M_2$AChR bound with atropine.

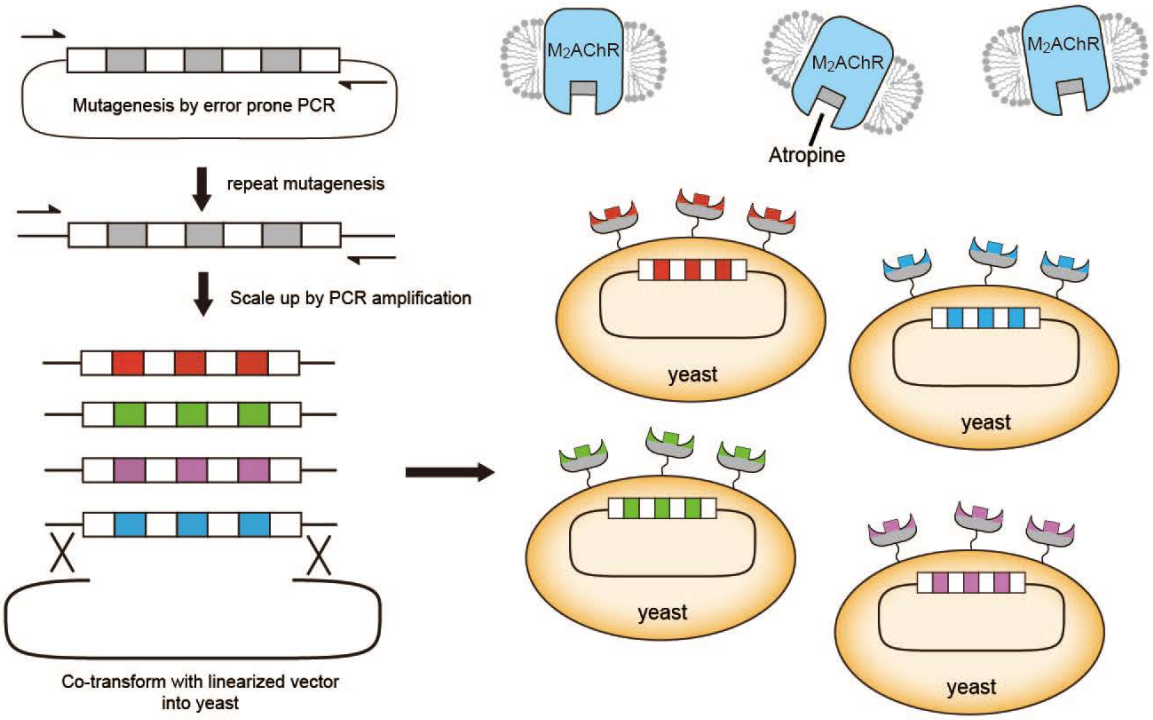


**Fig. S9.** A yeast surface display library was generated by error-prone PCR. In order to introduce large number of mutations in a short fragment of clone24, the error-prone PCR was repeated using the product of the first PCR as a template. The product of the second error-prone PCR was upscaled and co-transformed into yeast to generate a yeast library and used against $M_2$AChR bound with atropine.

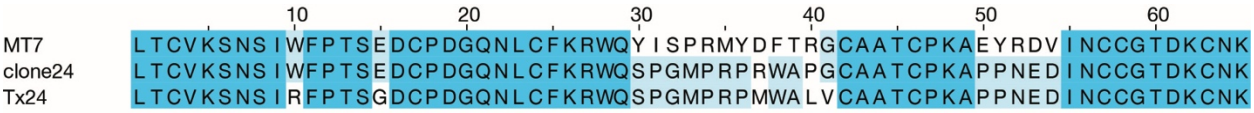


**Fig. S10.** Amino-acid sequence alignment of MT7, clone24, and Tx24. Residue numbers are represented above the alignment. Amino-acid residues highlighted in blue and pale-blue represent the perfect and partial conservation among these three proteins, respectively.

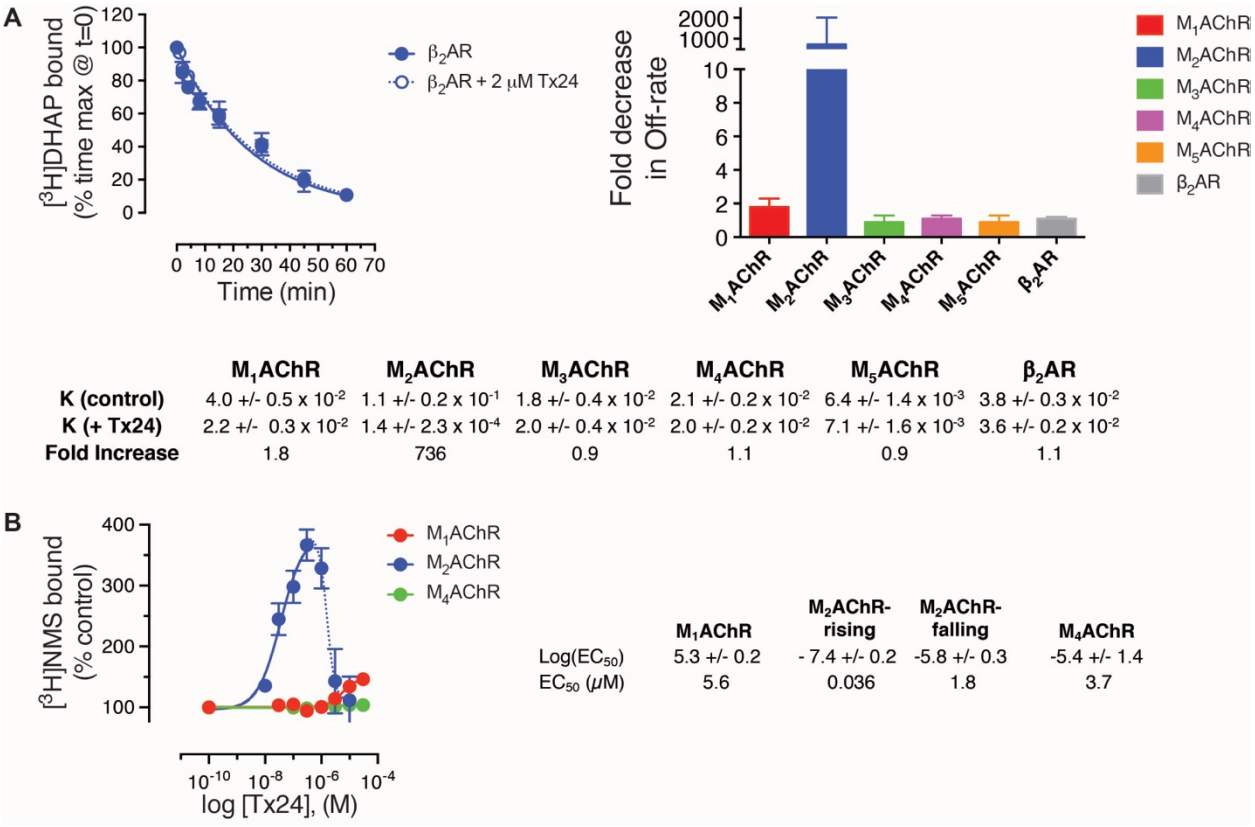


**Fig. S11. (A)** (Left) [$^3$H]DHAP dissociation from $\beta_2$AR in the absence (filled symbols, solid line), or presence (empty symbol, dotted line) of 2 μM Tx24. Shown are the combined results from 4 assays performed in duplicate. (Right, bottom) Summary of dissociation kinetics of [$^3$H]NMS from $M_2$AChR, $M_1$AChR, $M_3$AChR, $M_4$AChR, $M_5$AChR, or [$^3$H]DHAP from $\beta_2$AR, in the absence or presence of 2 μM Tx24 as described in the Methods Section. Dissociation rate constants ($K_{off}$, min$^{-1}$) with or without Tx24 were determined using Prizm 6 (GraphPad LLC, San Diego CA) using a single phase exponential decay model (n=4). **(B)** The concentration-dependent effect of Tx24 on [$^3$H]NMS (0.3 nM) binding to $M_2$AChR (blue), $M_1$AChR (red) or $M_4$AChR (green). Data were fit to a logistics curve using Prizm 6 (GraphPad LLC, San Diego CA). For $M_2$AChR, the rising phase (solid line) of [$^3$H]NMS binding was fit separately from the falling phase (dotted line). Symbols and error bars represent mean and s.e.m., respectively of combined results from 4 assays performed in duplicate.

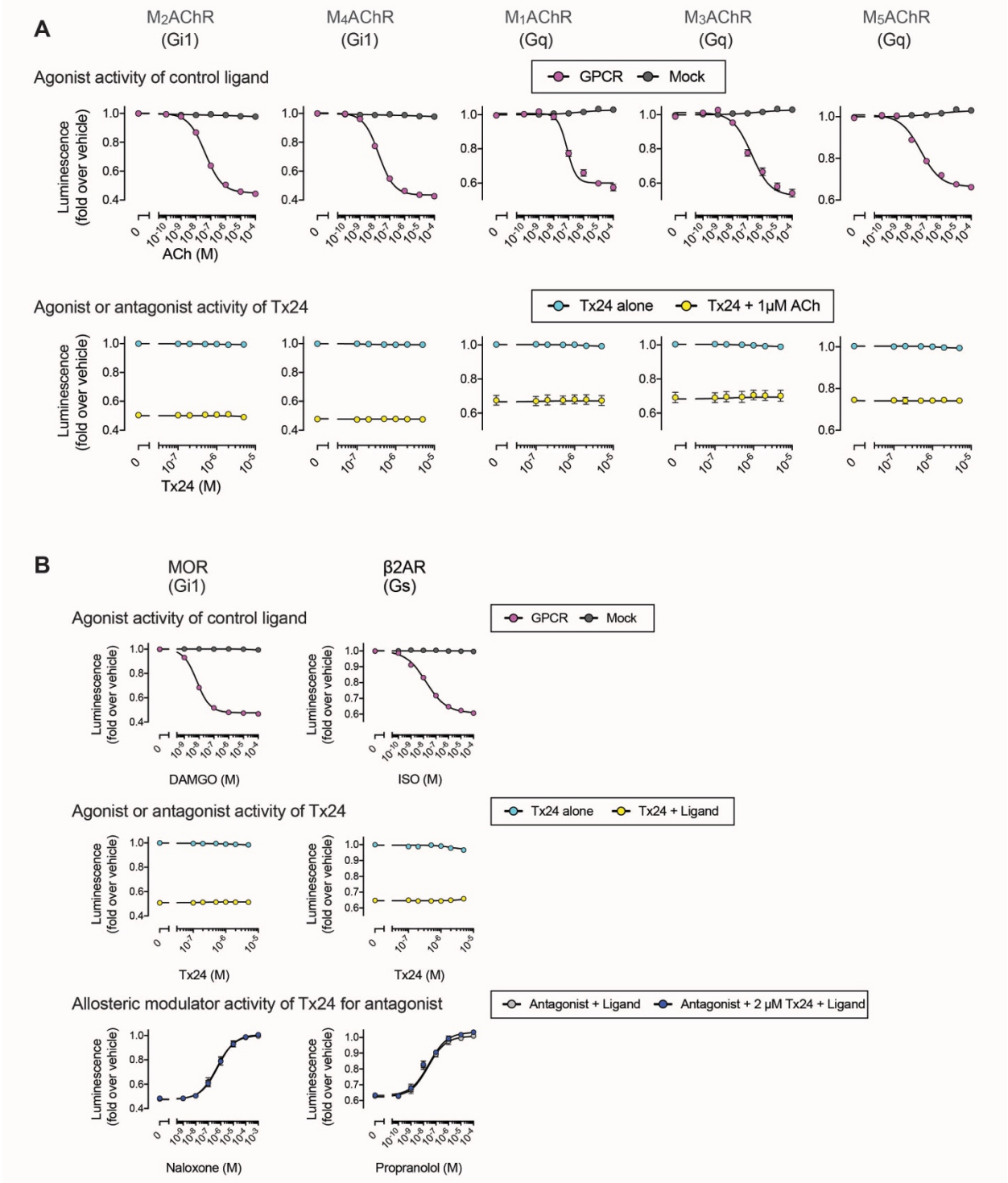
A
M2AChR (Gi1)
M4AChR (Gi1)
M1AChR (Gq)
M3AChR (Gq)
M5AChR (Gq)
Agonist activity of control ligand
GPCR
Mock
Luminescence (fold over vehicle)
ACh (M)
Agonist or antagonist activity of Tx24
Tx24 alone
Tx24 + 1μM ACh
Tx24 (M)
B
MOR (Gi1)
β2AR (Gs)
Agonist activity of control ligand
GPCR
Mock
DAMGO (M)
ISO (M)
Agonist or antagonist activity of Tx24
Tx24 alone
Tx24 + Ligand
Tx24 (M)
Allosteric modulator activity of Tx24 for antagonist
Antagonist + Ligand
Antagonist + 2 μM Tx24 + Ligand
Naloxone (M)
Propranolol (M)

**Fig. S12. (A)** Agonist activity of a control ligand acetylcholine (upper panels), and absence of agonistic or antagonistic activity of Tx24 for MAChRs (lower panels). HEK293 cells transiently expressing an indicated NanoBiT-G protein and a test MAChRs (or an empty vector; Mock) were loaded with coelenterazine and treated with a titrated ligand molecule. To measure antagonist activity, 1μM ACh was used as a stimulator (lower panels). Changes in luminescent signals were normalized to vehicle treatment and fitted to a four-parameter sigmoidal curve. **(B)** Absence of pharmacological activity of Tx24 for MOR and β2AR. The cells expressing the NanoBiT-G protein and the test GPCR or mock were treated with a control agonist (upper panels), titration of Tx24 (middle panel), or pretreated with antagonist and Tx24 followed by agonist stimulation (lower panel: 100 nM DAMGO for MOR; 100 nM Isoproterenol for β2AR). Symbols and error bars represent mean and s.e.m., respectively, of at least 3 independent experiments each performed in duplicate (also see Table S2).

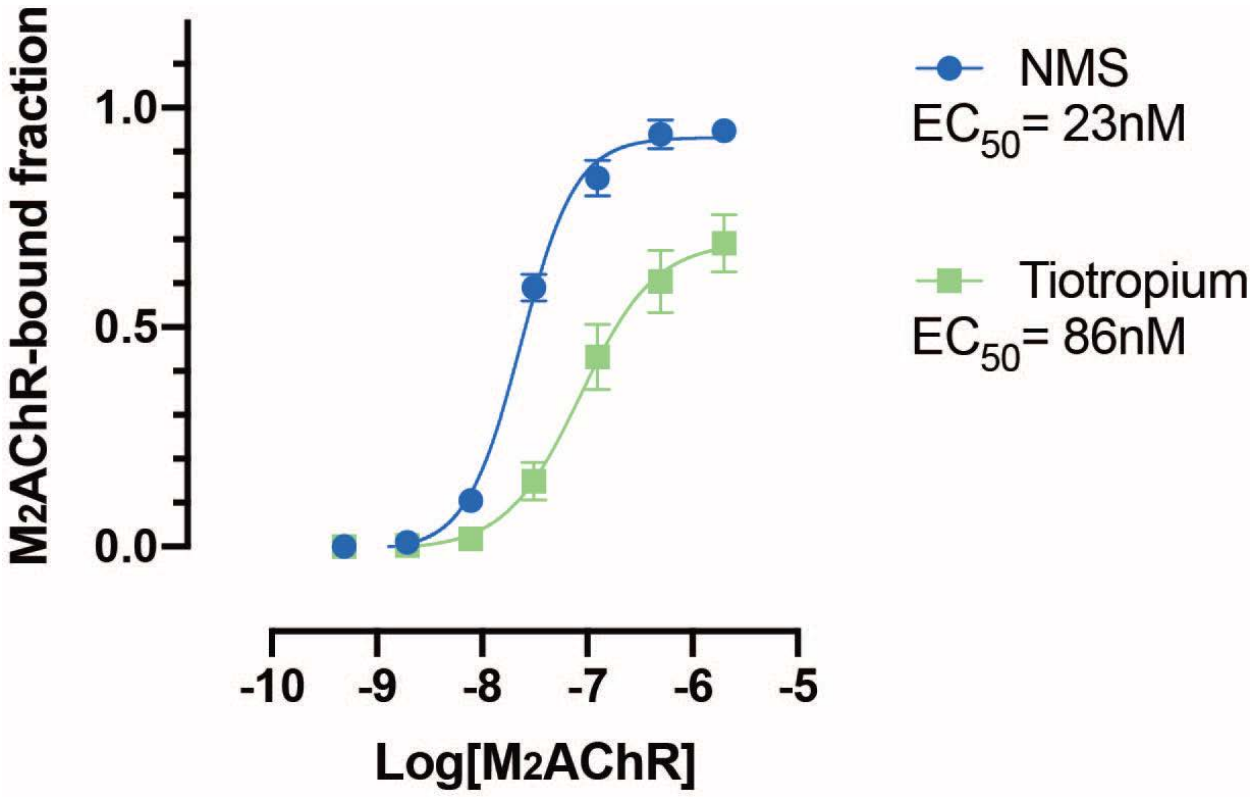


**Fig. S13.** On-yeast affinity measurement of Tx24 to $M_2$AChR bound with NMS or tiotropium. Yeast cells displaying Tx24 on the surface were incubated with $M_2$AChR bound with either NMS or tiotropium. Cells were washed to remove unbound $M_2$AChR followed by the surface staining with anti-FLAG antibody conjugated with Alexa-647. The fluorescence signal from the receptor-bound yeast population was analysed by flow cytometry. Data represents mean ± s.e.m. of three independent experiments.

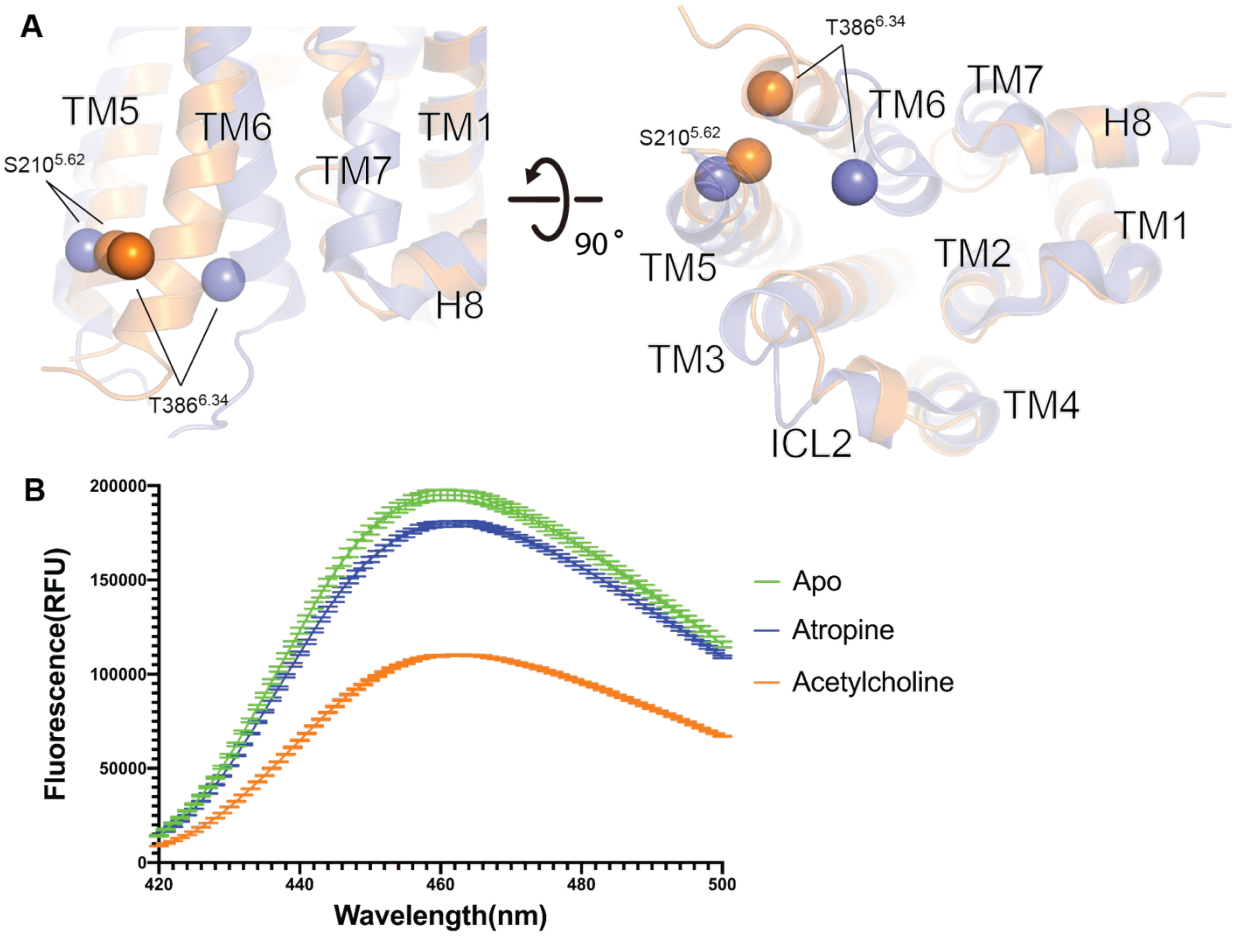


**Fig. S14.** Position of mBBr on $M_2$AChR and fluorescence spectra in the presence or absence of the ligands, atropine or acetylcholine. **(A)** Structural comparison of the inactive (blue, PDB ID: 3UON) and the active (orange: PDB ID: 4MQS) conformations of $M_2$AChR. Positions of Ser210$^{5.62}$ and Thr386$^{6.34}$, residues mutated to tryptophan and cystine, respectively, are labeled and represented as spheres. **(B)** mBBr fluorescence spectra of $M_2$AChR in apo-state, bound with atropine, and acetylcholine. Data represents mean signals with s.e.m. from at least three independent measurements.

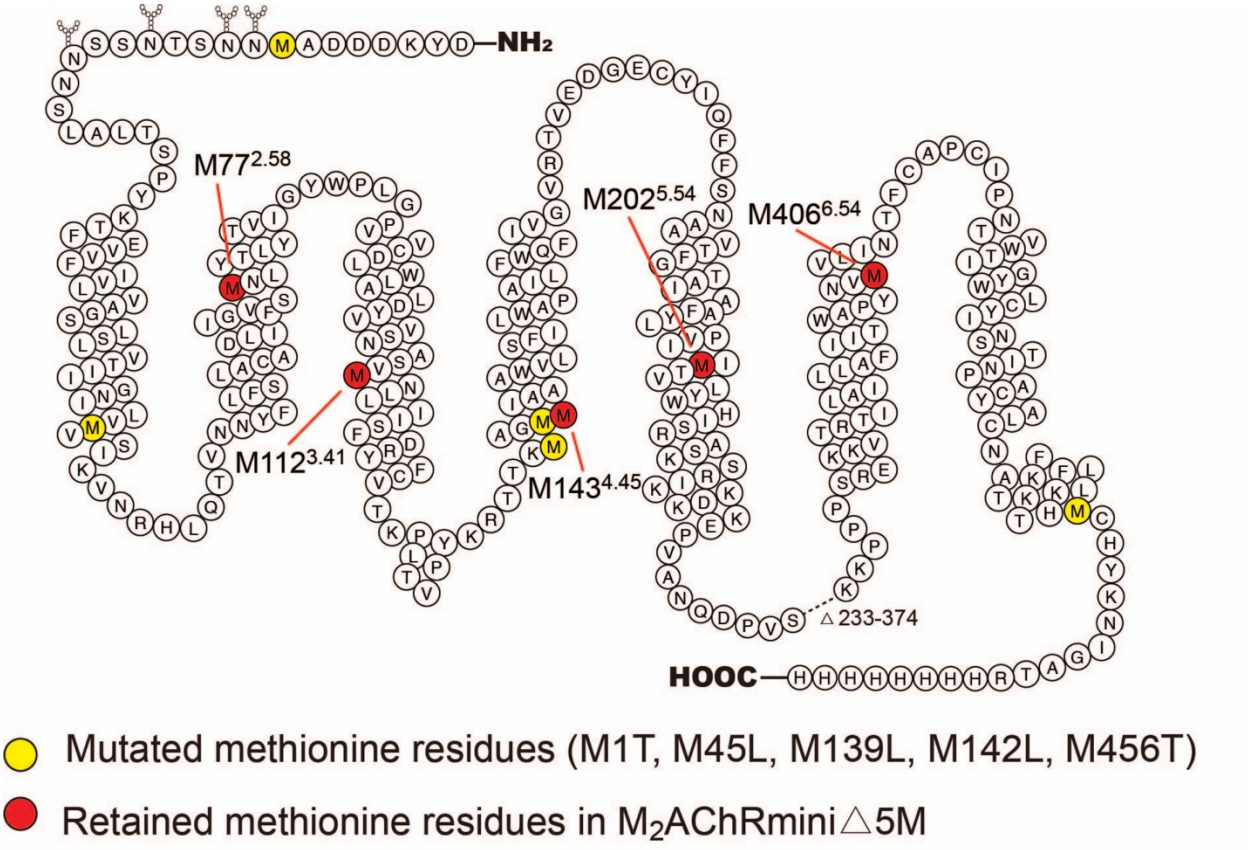


**Fig. S15.** A snake diagram of the $M_2$AChR construct used for the NMR experiments where the receptor was labeled with $^{13}CH_3$-ε-methionine. Five methionine residues were mutated to either threonine or leucine. The remaining 5 methionine residues distribute to TM2, TM3, TM4, TM5, and TM6, respectively.

## Table S1. Crystallographic data collection and refinement statistics.

| | $M_1$AChR-MT7 |
|---|---|
| **Beamline** | APS 23-ID-D (GM/CA) |
| **Resolution range** | 38.05 - 2.55 (2.64 - 2.55) |
| **Space group** | C 1 2 1 |
| **Unit cell** | 122.15 150.43 76.93 90 98.77 90 |
| **Total reflections** | 149892 (15597) |
| **Unique reflections** | 44411 (4440) |
| **Multiplicity** | 3.5 (3.5) |
| **Completeness (%)** | 99.26 (99.84) |
| **Mean I/sigma(I)** | 12.35 (1.18) |
| **Wilson B-factor** | 83.26 |
| **R-merge** | 0.040 (1.105) |
| **R-meas** | 0.046 (1.305) |
| **R-pim** | 0.026 (0.689) |
| **CC1/2** | 0.999 (0.659) |

| | |
|---|---|
| **CC*** | 1.000 (0.891) |
| **Reflections used in refinement** | 44346 (4436) |
| **Reflections used for R-free** | 1997 (200) |
| **R-work** | 0.245 (0.476) |
| **R-free** | 0.263 (0.468) |
| **CC(work)** | 0.918 (0.746) |
| **CC(free)** | 0.921 (0.727) |
| **Number of non-hydrogen atoms** | 4213 |
| **macromolecules** | 4041 |
| **ligands** | 165 |
| **Solvent** | 7 |
| **Protein residues** | 514 |
| **RMS(bonds)** | 0.002 |
| **RMS(angles)** | 0.53 |
| **Ramachandran favored (%)** | 98.04 |
| **Ramachandran allowed (%)** | 1.96 |

| | |
|---|---|
| **Ramachandran outliers (%)** | 0.00 |
| **Rotamer outliers (%)** | 0.00 |
| **Clashscore** | 7.34 |
| **Average B-factor** | 123.97 |
| **macromolecules** | 123.25 |
| **ligands** | 142.34 |
| **Solvent** | 103.33 |
| **Number of TLS groups** | 12 |

Statistics for the highest-resolution shell are shown in parentheses.

**Table S2. Pharmacological parameters for GPCR antagonists and Tx24**

| GPCR | Antagonist | Agonist | *n* = | $pIC_{50}$ Mean ± SEM | | |
|---|---|---|---|---|---|---|
| | | | | Vehicle | 2 µM Tx24 | |
| M2 | Atropine | 10 µM ACh | 3 | 6.91 ± 0.04 | 8.11 ± 0.09 | *** |
| M4 | Atropine | 10 µM ACh | 3 | 7.35 ± 0.05 | 7.37 ± 0.07 | NS |
| M1 | Atropine | 10 µM ACh | 3 | 7.73 ± 0.01 | 7.79 ± 0.01 | NS |
| M3 | Atropine | 10 µM ACh | 3 | 7.49 ± 0.05 | 7.52 ± 0.01 | NS |
| M5 | Atropine | 10 µM ACh | 3 | 7.63 ± 0.07 | 7.81 ± 0.07 | NS |
| MOR | Naloxone | 1 µM DAMGO | 3 | 6.25 ± 0.15 | 6.20 ± 0.21 | NS |
| β2AR | Propranolol | 1 µM ISO | 4 | 7.85 ± 0.08 | 7.75 ± 0.02 | NS |

***, $P < 0.001$; NS, not significantly different from non-Tx24 condition (vehicle) (Two-way ANOVA with Sidak multiple comparison test).

**Table S3. Pharmacological parameters for $M_2$AChR antagonists and Tx24**

| Antagonist | Tx24 | *n* = | $pIC_{50}$ Mean ± SEM | $IC_{50}$ | $\Delta pIC_{50}$ Mean ± SEM | | $\Delta IC_{50}$ | Log α Mean ± SEM | | α |
|---|---|---|---|---|---|---|---|---|---|---|
| Atropine | Vehicle | 4 | 7.26 ± 0.13 | 55 nM | 0 | | 1 | 0.75 ± 0.04 | *** | 5.6 |
| | 100 nM | 4 | 7.43 ± 0.10 | 37 nM | -0.17 ± 0.04 | ** | 0.67 | | | |
| | 500 nM | 4 | 7.94 ± 0.11 | 11 nM | -0.68 ± 0.03 | *** | 0.21 | | | |
| | 2 µM | 4 | 8.55 ± 0.13 | 2.8 nM | -1.29 ± 0.02 | *** | 0.051 | | | |
| NMS | Vehicle | 3 | 7.13 ± 0.02 | 74 nM | 0 | | 1 | 0.89 ± 0.04 | *** | 7.7 |
| | 100 nM | 3 | 7.41 ± 0.02 | 39 nM | -0.27 ± 0.01 | *** | 0.53 | | | |
| | 500 nM | 3 | 8.05 ± 0.05 | 8.9 nM | -0.92 ± 0.05 | *** | 0.12 | | | |
| | 2 µM | 3 | 8.51 ± 0.12 | 3.1 nM | -1.38 ± 0.12 | *** | 0.042 | | | |
| Tiotropium | Vehicle | 3 | 9.83 ± 0.18 | 0.15 nM | 0 | | 1 | 0.03 ± 0.02 | NS | 1.1 |
| | 100 nM | 3 | 9.83 ± 0.15 | 0.15 nM | 0.00 ± 0.04 | NS | 1.01 | | | |
| | 500 nM | 3 | 9.85 ± 0.17 | 0.14 nM | -0.01 ± 0.05 | NS | 0.98 | | | |
| | 2 µM | 3 | 9.86 ± 0.15 | 0.14 nM | -0.02 ± 0.05 | NS | 0.95 | | | |

**, P < 0.01; ***, P < 0.001; NS, not significantly different from non-Tx24 condition (vehicle)

(Two-way ANOVA with Sidak multiple comparison test).

**References and Notes**


1. S.-M. Lee, J. M. Booe, A. A. Pioszak, Structural insights into ligand recognition and selectivity for classes A, B, and C GPCRs. *Eur. J. Pharmacol.* **763**, 196–205 (2015). doi:10.1016/j.ejphar.2015.05.013 Medline

2. A. Christopoulos, Advances in G protein-coupled receptor allostery: From function to structure. *Mol. Pharmacol.* **86**, 463–478 (2014). doi:10.1124/mol.114.094342 Medline

3. C. J. Langmead, A. Christopoulos, Functional and structural perspectives on allosteric modulation of GPCRs. *Curr. Opin. Cell Biol.* **27**, 94–101 (2014). doi:10.1016/j.ceb.2013.11.007 Medline

4. P. Kessler, P. Marchot, M. Silva, D. Servent, The three-finger toxin fold: A multifunctional structural scaffold able to modulate cholinergic functions. *J. Neurochem.* **142** (suppl. 2), 7–18 (2017). doi:10.1111/jnc.13975 Medline

5. I. Ségalas, C. Roumestand, S. Zinn-Justin, B. Gilquin, R. Ménez, A. Ménez, F. Toma, Solution structure of a green mamba toxin that activates muscarinic acetylcholine receptors, as studied by nuclear magnetic resonance and molecular modeling. *Biochemistry* **34**, 1248–1260 (1995). doi:10.1021/bi00004a019 Medline

6. J. S. Liang, J. Carsi-Gabrenas, J. L. Krajewski, J. M. McCafferty, S. L. Purkerson, M. P. Santiago, W. L. Strauss, H. H. Valentine, L. T. Potter, Anti-muscarinic toxins from Dendroaspis angusticeps. *Toxicon* **34**, 1257–1267 (1996). doi:10.1016/S0041-0101(96)00109-2 Medline

7. K. N. Bradley, Muscarinic toxins from the green mamba. *Pharmacol. Ther.* **85**, 87–109 (2000). doi:10.1016/S0163-7258(99)00064-9 Medline

8. E. Karlsson, M. Jolkkonen, E. Mulugeta, P. Onali, A. Adem, Snake toxins with high selectivity for subtypes of muscarinic acetylcholine receptors. *Biochimie* **82**, 793–806 (2000). doi:10.1016/S0300-9084(00)01176-7 Medline

9. D. Jerusalinsky, E. Kornisiuk, P. Alfaro, J. Quillfeldt, A. Ferreira, V. E. Rial, R. Durán, C. Cerveñansky, Muscarinic toxins: Novel pharmacological tools for the muscarinic cholinergic system. *Toxicon* **38**, 747–761 (2000). doi:10.1016/S0041-0101(99)00196-8 Medline

10. D. Servent, G. Blanchet, G. Mourier, C. Marquer, E. Marcon, C. Fruchart-Gaillard, Muscarinic toxins. *Toxicon* **58**, 455–463 (2011). doi:10.1016/j.toxicon.2011.08.004 Medline

11. D. Servent, C. Fruchart-Gaillard, Muscarinic toxins: Tools for the study of the pharmacological and functional properties of muscarinic receptors. *J. Neurochem.* **109**, 1193–1202 (2009). doi:10.1111/j.1471-4159.2009.06092.x Medline

12. S. I. Max, J. S. Liang, L. T. Potter, Purification and properties of m1-toxin, a specific antagonist of m1 muscarinic receptors. *J. Neurosci.* **13**, 4293–4300 (1993). doi:10.1523/JNEUROSCI.13-10-04293.1993 Medline

13. S. I. Max, J. S. Liang, L. T. Potter, Stable allosteric binding of m1-toxin to m1 muscarinic receptors. *Mol. Pharmacol.* **44**, 1171–1175 (1993). Medline

14. S. I. Max, J. S. Liang, H. H. Valentine, L. T. Potter, Use of m1-toxin as a selective antagonist of m1 muscarinic receptors. *J. Pharmacol. Exp. Ther.* **267**, 480–485 (1993). Medline

15. J. M. Carsi, L. T. Potter, m1-toxin isotoxins from the green mamba (Dendroaspis angusticeps) that selectively block m1 muscarinic receptors. *Life Sci.* **68**, 2541–2547 (2001). doi:10.1016/s0041-0101(99)00141-5

16. J. Näsman, M. Jolkkonen, S. Ammoun, E. Karlsson, K. E. O. Åkerman, Recombinant expression of a selective blocker of M(1) muscarinic receptors. *Biochem. Biophys. Res. Commun.* **271**, 435–439 (2000). doi:10.1006/bbrc.2000.2657 Medline

17. J. L. Krajewski, I. M. Dickerson, L. T. Potter, Site-directed mutagenesis of m1-toxin1: Two amino acids responsible for stable toxin binding to M(1) muscarinic receptors. *Mol. Pharmacol.* **60**, 725–731 (2001). Medline

18. M. C. Olianas, C. Maullu, A. Adem, E. Mulugeta, E. Karlsson, P. Onali, Inhibition of acetylcholine muscarinic M(1) receptor function by the M(1)-selective ligand muscarinic toxin 7 (MT-7). *Br. J. Pharmacol.* **131**, 447–452 (2000). doi:10.1038/sj.bjp.0703606 Medline

19. K. N. Bradley, E. G. Rowan, A. L. Harvey, Effects of muscarinic toxins MT2 and MT7, from green mamba venom, on m1, m3 and m5 muscarinic receptors expressed in Chinese hamster ovary cells. *Toxicon* **41**, 207–215 (2003). doi:10.1016/S0041-0101(02)00278-7 Medline

20. M. C. Olianas, A. Adem, E. Karlsson, P. Onali, Action of the muscarinic toxin MT7 on agonist-bound muscarinic M1 receptors. *Eur. J. Pharmacol.* **487**, 65–72 (2004). doi:10.1016/j.ejphar.2004.01.029 Medline

21. D. M. Thal, B. Sun, D. Feng, V. Nawaratne, K. Leach, C. C. Felder, M. G. Bures, D. A. Evans, W. I. Weis, P. Bachhawat, T. S. Kobilka, P. M. Sexton, B. K. Kobilka, A. Christopoulos, Crystal structures of the M1 and M4 muscarinic acetylcholine receptors. *Nature* **531**, 335–340 (2016). doi:10.1038/nature17188 Medline

22. C. Fruchart-Gaillard, G. Mourier, C. Marquer, E. Stura, N. J. M. Birdsall, D. Servent, Different interactions between MT7 toxin and the human muscarinic M1 receptor in its free and N-methylscopolamine-occupied states. *Mol. Pharmacol.* **74**, 1554–1563 (2008). doi:10.1124/mol.108.050773 Medline

23. B. Gilquin, M. Bourgoin, R. Ménez, M.-H. Le Du, D. Servent, S. Zinn-Justin, A. Ménez, Motions and structural variability within toxins: Implication for their use as scaffolds for protein engineering. *Protein Sci.* **12**, 266–277 (2003). doi:10.1110/ps.0227703 Medline

24. G. Blanchet, G. Collet, G. Mourier, N. Gilles, C. Fruchart-Gaillard, E. Marcon, D. Servent, Polypharmacology profiles and phylogenetic analysis of three-finger toxins from mamba venom: Case of aminergic toxins. *Biochimie* **103**, 109–117 (2014). doi:10.1016/j.biochi.2014.04.009 Medline

25. A. Kukkonen, M. Peräkylä, K. E. O. Åkerman, J. Näsman, Muscarinic toxin 7 selectivity is dictated by extracellular receptor loops. *J. Biol. Chem.* **279**, 50923–50929 (2004). doi:10.1074/jbc.M406424200 Medline

26. S. Rondinelli, K. Näreoja, J. Näsman, Molecular conversion of muscarinic acetylcholine receptor M(5) to muscarinic toxin 7 (MT7)-binding protein. *Toxins* **3**, 1393–1404 (2011). doi:10.3390/toxins3111393 Medline

27. C. Marquer, C. Fruchart-Gaillard, G. Letellier, E. Marcon, G. Mourier, S. Zinn-Justin, A. Ménez, D. Servent, B. Gilquin, Structural model of ligand-G protein-coupled receptor (GPCR) complex based on experimental double mutant cycle data: MT7 snake toxin bound to dimeric hM1 muscarinic receptor. *J. Biol. Chem.* **286**, 31661–31675 (2011). doi:10.1074/jbc.M111.261404 Medline

28. J. A. Ballesteros, H. Weinstein, in *Receptor Molecular Biology*, vol. 25 of *Methods in Neurosciences*, S. C. Sealfon, Ed. (Academic Press, 1995), pp. 366–428.

29. J. Xu, H. Zhao, Z. Zheng, Y. Wang, Y. Niu, H. Wang, J. Xu, Y. Lu, H. Chen, Structural determinants for the interactions between muscarinic toxin 7 and muscarinic acetylcholine receptors. *J. Mol. Recognit.* **28**, 239–252 (2015). doi:10.1002/jmr.2438 Medline

30. A. Abdul-Ridha, L. López, P. Keov, D. M. Thal, S. N. Mistry, P. M. Sexton, J. R. Lane, M. Canals, A. Christopoulos, Molecular determinants of allosteric modulation at the M1 muscarinic acetylcholine receptor. *J. Biol. Chem.* **289**, 6067–6079 (2014). doi:10.1074/jbc.M113.539080 Medline

31. A. Abdul-Ridha, J. R. Lane, S. N. Mistry, L. López, P. M. Sexton, P. J. Scammells, A. Christopoulos, M. Canals, Mechanistic insights into allosteric structure-function relationships at the M1 muscarinic acetylcholine receptor. *J. Biol. Chem.* **289**, 33701–33711 (2014). doi:10.1074/jbc.M114.604967 Medline

32. L. Ma, M. A. Seager, M. Wittmann, M. Jacobson, D. Bickel, M. Burno, K. Jones, V. K. Graufelds, G. Xu, M. Pearson, A. McCampbell, R. Gaspar, P. Shughrue, A. Danziger, C. Regan, R. Flick, D. Pascarella, S. Garson, S. Doran, C. Kreatsoulas, L. Veng, C. W. Lindsley, W. Shipe, S. Kuduk, C. Sur, G. Kinney, G. R. Seabrook, W. J. Ray, Selective activation of the M1 muscarinic acetylcholine receptor achieved by allosteric potentiation. *Proc. Natl. Acad. Sci. U.S.A.* **106**, 15950–15955 (2009). doi:10.1073/pnas.0900903106 Medline

33. S. A. Hollingsworth, B. Kelly, C. Valant, J. A. Michaelis, O. Mastromihalis, G. Thompson, A. J. Venkatakrishnan, S. Hertig, P. J. Scammells, P. M. Sexton, C. C. Felder, A. Christopoulos, R. O. Dror, Cryptic pocket formation underlies allosteric modulator selectivity at muscarinic GPCRs. *Nat. Commun.* **10**, 3289 (2019). doi:10.1038/s41467-019-11062-7 Medline

34. R. O. Dror, H. F. Green, C. Valant, D. W. Borhani, J. R. Valcourt, A. C. Pan, D. H. Arlow, M. Canals, J. R. Lane, R. Rahmani, J. B. Baell, P. M. Sexton, A. Christopoulos, D. E. Shaw, Structural basis for modulation of a G-protein-coupled receptor by allosteric drugs. *Nature* **503**, 295–299 (2013). doi:10.1038/nature12595 Medline

35. A. C. Kruse, A. M. Ring, A. Manglik, J. Hu, K. Hu, K. Eitel, H. Hübner, E. Pardon, C. Valant, P. M. Sexton, A. Christopoulos, C. C. Felder, P. Gmeiner, J. Steyaert, W. I. Weis, K. C. Garcia, J. Wess, B. K. Kobilka, Activation and allosteric modulation of a muscarinic acetylcholine receptor. *Nature* **504**, 101–106 (2013). doi:10.1038/nature12735 Medline

36. S. Maeda, Q. Qu, M. J. Robertson, G. Skiniotis, B. K. Kobilka, Structures of the M1 and M2 muscarinic acetylcholine receptor/G-protein complexes. *Science* **364**, 552–557 (2019). doi:10.1126/science.aaw5188 Medline

37. I. Visiers, J. A. Ballesteros, H. Weinstein, Three-dimensional representations of G protein-coupled receptor structures and mechanisms. *Methods Enzymol.* **343**, 329–371 (2002). doi:10.1016/S0076-6879(02)43145-X Medline

38. M. Naimuddin, S. Kobayashi, C. Tsutsui, M. Machida, N. Nemoto, T. Sakai, T. Kubo, Directed evolution of a three-finger neurotoxin by using cDNA display yields antagonists as well as agonists of interleukin-6 receptor signaling. *Mol. Brain* **4**, 2 (2011). doi:10.1186/1756-6606-4-2 Medline

39. W. Cai, M. Naimuddin, H. Inagaki, K. Kameyama, N. Ishida, T. Kubo, Directed evolution of three-finger toxin to produce serine protease inhibitors. *J. Recept. Signal Transduct.* **34**, 154–161 (2014). doi:10.3109/10799893.2013.865747 Medline

40. A. Inoue, F. Raimondi, F. M. N. Kadji, G. Singh, T. Kishi, A. Uwamizu, Y. Ono, Y. Shinjo, S. Ishida, N. Arang, K. Kawakami, J. S. Gutkind, J. Aoki, R. B. Russell, Illuminating G-Protein-Coupling Selectivity of GPCRs. *Cell* **177**, 1933–1947.e25 (2019). doi:10.1016/j.cell.2019.04.044 Medline

41. C. Valant, C. C. Felder, P. M. Sexton, A. Christopoulos, Probe dependence in the allosteric modulation of a G protein-coupled receptor: Implications for detection and validation of allosteric ligand effects. *Mol. Pharmacol.* **81**, 41–52 (2012). doi:10.1124/mol.111.074872 Medline

42. J. Xu, Y. Hu, J. Kaindl, P. Risel, H. Hübner, S. Maeda, X. Niu, H. Li, P. Gmeiner, C. Jin, B. K. Kobilka, Conformational Complexity and Dynamics in a Muscarinic Receptor Revealed by NMR Spectroscopy. *Mol. Cell* **75**, 53–65.e7 (2019). doi:10.1016/j.molcel.2019.04.028 Medline

43. E. Muratspahić, M. Freissmuth, C. W. Gruber, Nature-Derived Peptides: A Growing Niche for GPCR Ligand Discovery. *Trends Pharmacol. Sci.* **40**, 309–326 (2019). doi:10.1016/j.tips.2019.03.004 Medline

44. S. Yasuda, Y. Kajiwara, Y. Toyoda, K. Morimoto, R. Suno, S. Iwata, T. Kobayashi, T. Murata, M. Kinoshita, Hot-Spot Residues to be Mutated Common in G Protein-Coupled Receptors of Class A: Identification of Thermostabilizing Mutations Followed by Determination of Three-Dimensional Structures for Two Example Receptors. *J. Phys. Chem. B* **121**, 6341–6350 (2017). doi:10.1021/acs.jpcb.7b02997 Medline

45. W. Kabsch, XDS. *Acta Crystallogr. D* **66**, 125–132 (2010). doi:10.1107/S0907444909047337 Medline

46. P. R. Evans, G. N. Murshudov, How good are my data and what is the resolution? *Acta Crystallogr. D* **69**, 1204–1214 (2013). doi:10.1107/S0907444913000061 Medline

47. A. J. McCoy, R. W. Grosse-Kunstleve, P. D. Adams, M. D. Winn, L. C. Storoni, R. J. Read, Phaser crystallographic software. *J. Appl. Crystallogr.* **40**, 658–674 (2007). doi:10.1107/S0021889807021206 Medline

48. P. D. Adams, P. V. Afonine, G. Bunkóczi, V. B. Chen, I. W. Davis, N. Echols, J. J. Headd, L.-W. Hung, G. J. Kapral, R. W. Grosse-Kunstleve, A. J. McCoy, N. W. Moriarty, R. Oeffner, R. J. Read, D. C. Richardson, J. S. Richardson, T. C. Terwilliger, P. H. Zwart, PHENIX: A comprehensive Python-based system for macromolecular structure solution. *Acta Crystallogr. D* **66**, 213–221 (2010). doi:10.1107/S0907444909052925 Medline

49. P. Emsley, B. Lohkamp, W. G. Scott, K. Cowtan, Features and development of Coot. *Acta Crystallogr. D* **66**, 486–501 (2010). doi:10.1107/S0907444910007493 Medline

50. X. Yao, C. Parnot, X. Deupi, V. R. P. Ratnala, G. Swaminath, D. Farrens, B. Kobilka, Coupling ligand structure to specific conformational switches in the beta2-adrenoceptor. *Nat. Chem. Biol.* **2**, 417–422 (2006). doi:10.1038/nchembio801 Medline

51. F. Delaglio, S. Grzesiek, G. W. Vuister, G. Zhu, J. Pfeifer, A. Bax, NMRPipe: A multidimensional spectral processing system based on UNIX pipes. *J. Biomol. NMR* **6**, 277–293 (1995). doi:10.1007/BF00197809 Medline

52. B. A. Johnson, R. A. Blevins, NMR View: A computer program for the visualization and analysis of NMR data. *J. Biomol. NMR* **4**, 603–614 (1994). doi:10.1007/BF00404272 Medline

53. M. Korczynska, M. J. Clark, C. Valant, J. Xu, E. Von Moo, S. Albold, D. R. Weiss, H. Torosyan, W. Huang, A. C. Kruse, B. R. Lyda, L. T. May, J.-A. Baltos, P. M. Sexton, B. K. Kobilka, A. Christopoulos, B. K. Shoichet, R. K. Sunahara, Structure-based discovery of selective positive allosteric modulators of antagonists for the $M_2$ muscarinic acetylcholine receptor. *Proc. Natl. Acad. Sci. U.S.A.* **115**, E2419–E2428 (2018). doi:10.1073/pnas.1718037115 Medline